

# Energy dependence of a Low Frequency QPO in GRS 1915+105

J. Rodriguez<sup>1</sup>, Ph. Durouchoux<sup>1</sup>, I. F. Mirabel<sup>1,2</sup>, Y. Ueda<sup>3</sup>, M. Tagger<sup>1</sup>, and K. Yamaoka<sup>4</sup>

<sup>1</sup> DSM/DAPNIA/Service d'Astrophysique (CNRS URA 2052), CEA Saclay, 91191 Gif-sur-Yvette, France,

<sup>2</sup> Instituto de Astronomía y Física del Espacio/CONICET, Buenos Aires, Argentina,

<sup>3</sup> Institute of Space and Astronautical Science, Yoshinodai 3-1-1, Sagamihara, Kanagawa 229-8510, Japan,

<sup>4</sup> RIKEN The Institute of Physical and Chemical Research, Hirosawa 2-1, Wako, Saitama 351-0198, Japan.

Received date; Accepted date

**Abstract.** We analyze a set of three RXTE Target of Opportunity observations of the Galactic microquasar GRS 1915+105, observed on April 2000, during a multi-wavelength campaign. During the three observations, a strong, variable low frequency (2 – 9 Hz) quasi periodic oscillation (hereafter QPO), often referred to as the ubiquitous QPO, is detected together with its first harmonic.

We study the spectral properties of both features, and show that : 1) their frequency variations are better correlated with the soft X-ray flux (2 – 5 keV), favoring thus the location of the QPO in the accretion disk; 2) the QPO affects more the hard X-rays, usually taken as the signature of an inverse compton scattering of the soft photons in a corona; 3) the fundamental and its harmonic do not behave in the same manner: the fundamental sees its power increase with the energy up to 40 keV, whereas the harmonic increases up to  $\sim 10$  keV.

The results presented here could find an explanation in the context of the Accretion-Ejection Instability, which could appear as a rotating spiral or hot point located in the disk, between its innermost edge and the corotation radius. The presence of the harmonic could then be a signature of the non-linear behavior of the instability. The high-energy ( $> 40$  keV) decrease of the fundamental would favor an interpretation where most or all of the quasi-periodic modulation at high energies comes, not from the comptonized corona as usually assumed, but from a hot point in the optically thick disk.

**Key words.** Quasi Periodic Oscillations - Microquasar - X-Ray observation - Stars : individual GRS 1915+105

## 1. Introduction

X-ray binaries exhibit strong X-ray emission, from the soft ( $\sim 0.1$  keV) to the hard X-rays (up to a few hundred keV), sometimes up to the MeV domain. The emission processes are thought to occur in the close vicinity of a stellar-mass compact object (either a Neutron Star or a Black Hole), the soft part of the spectrum being usually taken as the thermal emission of an accretion disk, whereas the hard part is thought to be the manifestation of an inverse compton scattering of the soft photons, with relativistic electrons present in a hot coronal medium. The sources may be distinguished by several characteristics, such as the companion mass, whenever this latter is known, the shape of their spectra, or by the presence of strong collimated ejecta. In the latter case, the similarity with AGN led to the definition of microquasars (Mirabel *et al.*, 1992), some of them known to be sources with superluminal jets (Mirabel & Rodríguez, 1999).

GRS 1915+105 has first been discovered as a Soft X-ray Transient by WATCH on board *GRANAT* (Castro-Tirado *et al.*, 1992), and then identified as the first Galactic source to have ejections with apparent superluminal motion (Mirabel & Rodríguez, 1994). The distance to the source has been estimated to 12.5 kpc, its inclination  $\sim 70^\circ$ , and the velocity of the jet  $0.92c$  (Mirabel & Rodríguez, 1994). Since then, the source has been observed with many X-ray satellites, and its spectrum is typical of that of Black Hole Candidates (BHC), such as GRO J1655–40. Only recently, however, the spectral type of the companion has been identified as a K–M III star (Greiner *et al.*, 2001), classifying the source as a low mass X-ray binary. The mass of the primary has been estimated to  $14 \pm 4 M_\odot$  (Greiner, Cuby & McCaughrean, 2001), confirming the black hole nature of the compact object.

With the launch of the Rossi X-ray Timing Experiment (RXTE), and the excellent timing capacities of both its pointed instruments, the *Proportional Counter Array* (PCA) and the *High Energy X-ray Timing Experiment*

---

Send offprint requests to: J. Rodriguez  
(rodrigue@discovery.saclay.cea.fr)

(HEXTE), many X-ray Binaries and GRS 1915+105 in particular, have been discovered to exhibit Quasi Periodic Oscillations (QPOs), in several ranges of frequency (a few mHz up to hundred, and kilohertz in the case of neutron star primary). Though no physical explanation has yet been widely accepted, the QPOs are thought to occur in the close vicinity of the compact object.

Furthermore, it has been pointed out by Psaltis *et al.* (1999), that the QPOs could represent the same type of variability in both neutron stars and black hole systems, constraining the theoretical models, and giving important clues to the physics of these phenomena. In particular the study of QPOs should give important informations on the accretion flow, and thus on the physics of the disk. The detection of several types of QPOs can be attributed to different mechanisms, depending in particular on the source spectral state.

We will only focus here on the strong  $\sim 0.5 - 10$  Hz QPO, present during the low/hard spectral state of GRS 1915+105, often called “ubiquitous”, since it is nearly always present in that state and often observed in other Black Hole Binaries (e.g. XTE J1550–564, or GRO J1655–40). In that case, several authors have pointed out correlations between the frequency of the oscillations and some of the spectral parameters, such as the flux (Swank *et al.*, 1997; Markwardt *et al.*, 1999), the temperature of the disk (Muno *et al.*, 1999), and the disk color radius (Rodriguez *et al.*, 2002).

All these correlations constrained the location of the QPO in or close to the disk, and the systematic study of the QPO parameters should lead to a better understanding of the accretion and ejection mechanisms, thought to occur in this region.

Recently a new mechanism has been proposed by Tagger & Pellat (1999), to extract energy and angular momentum from the inner regions of the disk (permitting, thus the accretion) and transport them toward the corotation radius of the spiral wave formed in the disk, where they can be emitted directly toward the corona (Tagger & Pellat, 1999; Varnière & Tagger, 2001).

It has been shown by Rodriguez *et al.* (2001), and Varnière *et al.* (2002), that this model could explain the different frequency vs. radius correlations observed in GRO J1655–40 compared to GRS 1915+105 or (as had been found by Sobczak *et al.*, 1999) XTE J1550–564.

This model could also explain the correlations found by Mirabel *et al.* (1998), Eikenberry *et al.* (1998), Ueda *et al.* (2002, our observations being part of this latter work) during the  $\sim 30$  min cycle (Tagger, 1999 for a possible scenario), between X-ray light curves and the infrared and radio emissions, considered as the synchrotron signatures of an expanding ejected blob of material, relating then the energy needed to accelerate those blobs, to the one extracted from the accretion.

We present here observations of the source taken as a RXTE Target of Opportunity, in April 2000. In section 2 we present the data reduction and analysis methods used;

in section 3, we examine the first of the three observations, which is the most variable one, and focus then on the dynamical properties of the source, observed in different energy ranges. In section 4 we study the data of the following observations, where the source is much more steady, and thus, more adapted to extract the QPO parameters with high accuracy; we will interpret our observations in the last part of this paper.

## 2. Data reduction and analysis

The source has been observed on April 17<sup>th</sup>, 22<sup>nd</sup> and 23<sup>rd</sup>, 2000 as a target of opportunity. We have reduced and analyzed the processed data using the FTOOLS package (update 5.04). Observations IDs, exact time intervals, and dates are shown in table 1.

We first extracted, for the three observations, lightcurves covering the entire PCA energy range, from binned data with  $2^{-7}$  s = 7.8125 ms resolution, and event data with  $2^{-16}$  s = 15.25878  $\mu$ s, which were rebinned during the extraction process to 7.8125 ms.

In all cases, lightcurves were extracted from all the PCUs that were simultaneously turned “on” over a single interval (*i.e.* 5 on Apr. 17<sup>th</sup>, and 22<sup>nd</sup> first interval, four during the two following intervals that day, and three on Apr. 23<sup>rd</sup>). We combined all PCUs and all layers to get the most possible incoming flux. The exact PCA configuration over each interval is given in table 1.

“Good Time Intervals” (GTIs) were defined when the elevation angle was above  $10^\circ$ , the offset pointing less than  $0.02^\circ$ , and we also excluded the data taken while crossing the SAA.

Background lightcurves were generated using the PCABACKEST tool, from standard2 data, and subtracted from the raw lightcurves. We then generated power spectra and dynamical power spectra (hereafter DPS) using POWSPEC 1.0, calculating each FFT over  $\sim 4$  s time intervals (2048 bins in each intervals), and averaging then the result over 4 intervals. The resultant DPS has a resultant time bin  $\sim 16$  s, comparable to the time resolution of the standard 2 lightcurves. To follow the evolution of the QPOs parameters with the energy, we extracted, in the same standard way, lightcurves in five PCA energy channels: absolute channel 0 – 11 (in Matrix epoch4 corresponding to  $< 2 - 4.99$  keV), channel 12 – 29 (4.99 – 12.68 keV), channel 30 – 46 (12.68 – 20.06 keV), channel 47 – 89 (20.06 – 39.29 keV), channel 90 – 174 (39.29 – 80.04 keV). We then produced DPS and power spectra, as explained above, in each energy range.

## 3. First Observation : on April 17<sup>th</sup>

We extracted from both instruments standard lightcurves with 16 s time resolution, using the standard PCA and HEXTE reduction steps, for this observation; they are plotted on figure 1.

Date	MJD	Obs Id	Interval #	Time start (UT)	Time stop (UT)	PCUs "On"
04 17 2000	51651	50405 - 01 - 01 - 00	1	12h52m15s	13h42m55s	0 - 4
			2	14h27m43s	15h18m39s	0 - 4
04 22 2000	51656	50405 - 01 - 02 - 00	1	09h21m35s	10h15m27s	0 - 4
		50405 - 01 - 02 - 01	2	10h55m59s	11h38m07s	0, 2 - 4
		50405 - 01 - 02 - 02	3	12h31m59s	13h14m07s	0, 2 - 4
04 23 2000	51657	50405 - 01 - 03 - 00	1	07h40m31s	08h35m27s	0, 2, 3
			2	09h16m15s	09h59m59s	0, 2, 3

**Table 1.** List of the Observations reduced; the interval time are those define by the PCA good time intervals as defined in section 2. Relative time zero corresponds to 12h52m15s, start of the good time interval for interval # 1.

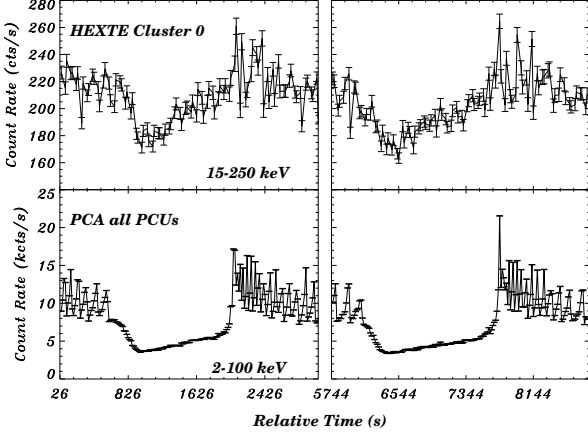


**Fig. 1.** The source on April 17<sup>th</sup>. Standard lightcurves covering in both cases the entire instrument energy range ( $\sim 15-250$  keV for HEXTE, and  $\sim 2-100$  keV for PCA); *Upper Panel* : HEXTE Cluster 0 standard lightcurves with 16 s time bins, *Lower Panel* : PCA standard 2 lightcurves with 16 s time bins. X axis is in unit of s; Y axis is in unit of cts/s (upper panels), and kcts/s (lower ones). Error bars are  $1\sigma$  statistical errors.

The source is in a  $\alpha$  state as defined by Belloni *et al.* (2000). PCA dynamical power spectra, covering the entire PCA energy range ( $\sim 2-100$  keV), are shown on figure 2 together with the PCA lightcurves.

The source presents large flux variations on short time scales ( $\sim 100$  s), together with a single QPO whose frequency has a similar behavior (figure 2). Then around time  $\sim 600$  s (first interval), and  $\sim 6000$  s (second), a large  $\sim 1000$ s dip occurs (figure 1). During that time, the QPO frequency varies from 9 Hz to 2.25 Hz, and a strong second QPO appears with a frequency  $\sim$  twice that of the fundamental, following the same frequency variations (figure 2). Then around relative time 2032 s (first interval), and 7716 s (second interval), a sudden and large soft X-ray spike, reaching  $\sim 4.8\times$  (respectively  $\sim 6.4\times$ ) the dip minimum flux, for the first (respectively second) interval, occurs and the source returns to a state similar to the one before the dip. Here the harmonic disappears, while the fundamental returns to a larger frequency and behaves as before the dip. In addition we show in fig. 3, DPS in the

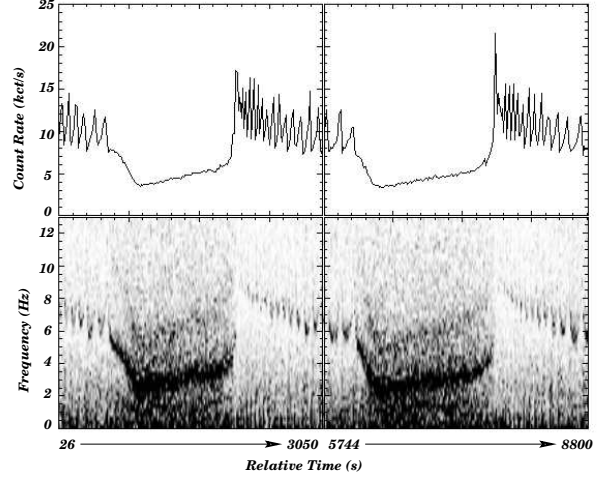


**Fig. 2.** PCA Lightcurve of the source during the whole observation; *Lower Panel* : Dynamical power spectra of the source on April 17<sup>th</sup>; the gap in the data corresponds to occultation due to the orbit. X axis is the relative time (time 0 is defined in table 1), in units of s. Y axis is in kcts/s (upper panels), and in Hz (lower ones).

five energy ranges defined in section 2, together with the corresponding lightcurves. One can immediately see that above 20 keV the harmonic is absent or very faint, and that above 40 keV (probably due to the high noise) the QPO disappears. We also see on figure 3 the evolution of the flux variations with the energy; the large dip seems to be smoothed with the energy.

We extracted from the soft lightcurves the relative time and the value of the flux of the peak occurring just before the dip (relative time 554 s, for the first interval, and 6064, for the second one); we then re-did the same procedure for the minimum of the dip (relative time 954 s for the first interval, and 6368 s for the second one), and we thus could estimate the relative amplitude of the variation of the flux, at the time where, also, the fundamental QPO sees its frequency varying from 9 to 2.25 Hz. We did this in each energy range, at the same times (allowing a maximum of two bins ( $\sim \pm 32$  s) of difference between each range). Results are shown in table 2.

Note that the soft spike corresponds in the higher energy range (above 20 keV) to a sudden decrease of the flux,

Energy Range (keV)	Variation Rate Interval # 1 (%)	Variation Rate Interval # 2 (%)
2–5	$72.95 \pm 0.63$	$71.19 \pm 0.66$
5–13	$70.24 \pm 0.61$	$69.61 \pm 0.63$
13–20	$47.84 \pm 1.78$	$42.37 \pm 1.88$
20–40	$22.18 \pm 4.26$	$21.29 \pm 4.07$

**Table 2.** Variations of the flux with the energy, between the last peak before the dip, and the bottom of the dip for the two intervals of April 17.

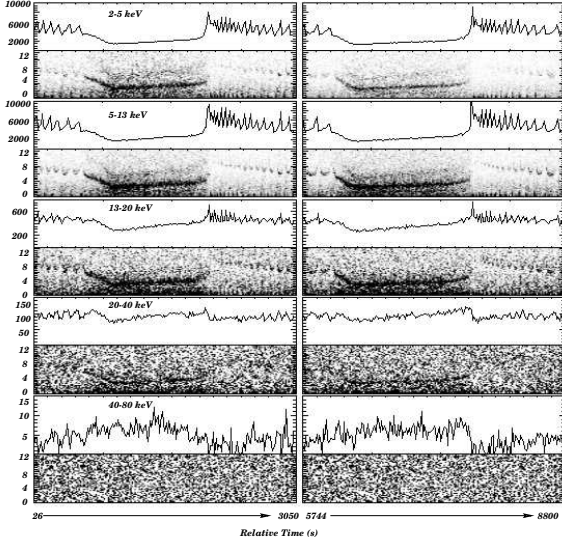


**Fig. 3.** Dynamical power spectra of the source on April 17<sup>th</sup> in the five PCA energy ranges; X axis in all cases are the time, covering relative time from 24 s to 3050 s (Left), and relative time from 5744 s to 8800 s (Right); upper panels are the standard 2 lightcurves in the indicated energy ranges. Y axis are in units of kcts/s for the upper panels, and in units of Hz for the lower ones.

indicating the cooling, or the disappearance of a part of the corona (multi-wavelength results can be found in Ueda *et al.*, 2002).

#### 4. Second and Third Observation : April 22<sup>nd</sup> and 23<sup>rd</sup>

As the lightcurves and dynamical power spectra did not present variations as strong as on the previous date, we did not focus here on the dynamical evolution of the QPO, but we just tried to correlate the QPO parameters with the energy range. Figure 4 shows the lightcurves with the dynamical power spectra from all the GTIs of both observations. The source is in a  $\chi$  state of Belloni *et al.*, 2000, characterized by a steady flux.

Power spectra covering the entire PCA range, shown on figure 5, are fitted with a model consisting of two broad lorentzians (continuum), plus sharper ones, modeling the QPO features. When the presence of the QPOs was not obvious, we estimated the parameters by freezing the lorentzian centroid frequency to the value found in the other energy ranges, and allowing both the width and the

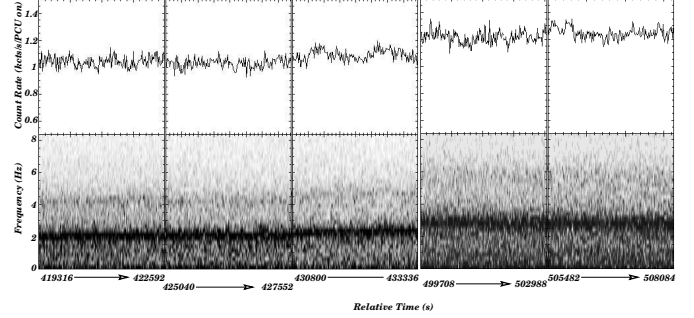


**Fig. 4.** Plot of the 16s PCA lightcurves (upper panel), and the dynamical power spectra (bottom), covering the three good time intervals of April 22<sup>nd</sup> (left Panel) and April 23<sup>rd</sup> (Right Panel). Once again time zero is April 17<sup>th</sup> good time interval start. Y axis of upper panels is in unit of kcts/s/PCU-on (see table 1 for the PCA configuration over each interval), while that of lower panels is in Hz.

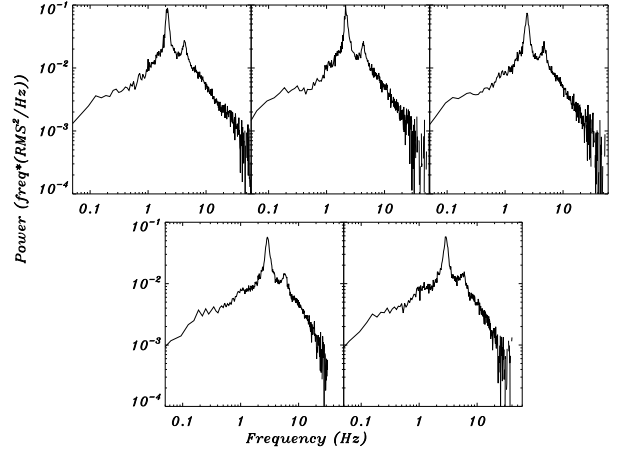


**Fig. 5.** Power spectra of the source on April 22<sup>nd</sup> (up), and April 23<sup>rd</sup> (lower panel). Y axis is the power in terms of  $Freq * RMS^2 / Hz$ , while X axis are the frequencies.

power to vary. In the case of the 40 – 80 keV range, since the statistics from single interval was poor, we chose to merged the observations where the QPO frequency was found to be close, i.e. intervals #1 and #2 from April 22, and intervals #1 and #2 from April 23; interval #3 from April 22 was fitted alone. Results from the fits for all the energy ranges defined in section 2 are shown in table 3. No variations similar to those of April 17 are present here; the flux remains fairly constant around a mean value 1050 cts/s/PCU-on, for the April 22 two first intervals, rising

slowly to  $\sim 1100$  cts/s/PCU-on, for the April 22 third interval, and reaching  $\sim 1200$  cts/s/PCU-on, on April 23. As expected, in the same time intervals the fundamental QPO sees its frequency slowly increase with time from  $\sim 2.14$  Hz (on Apr. 22) to  $\sim 2.9$  Hz (on Apr. 23) (figure 4, and table 3). The harmonic is still present during the five intervals, with a frequency varying from  $\sim 4.3$  Hz (on Apr. 22), to  $\sim 5.8$  Hz on April 23 first interval.

We plotted in figure 7 the evolution of the QPO power vs. energy range for the five GTIs. The upper points represent the behavior of the fundamental QPO, and the lower that of the harmonic; we can see that the power of the fundamental increases up to 40 keV, and then seems to decrease, whereas that of the harmonic seems to peak between the 5 – 13 and 13 – 20 keV ranges. Figure 6 repre-

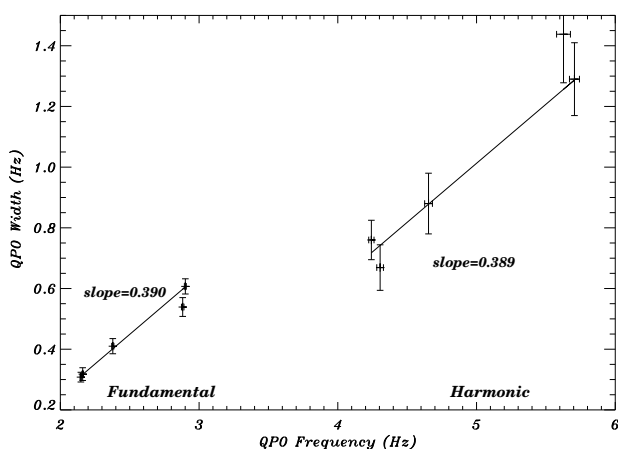


**Fig. 6.** Plot of QPO FWHM vs. QPO Frequency, for the five intervals covering Apr. 22<sup>nd</sup> and 23<sup>rd</sup>. Both axis are in units of Hz. In the two case the solid lines represent the best fit. The slopes are indicated in each cases.

sents the evolution of the QPOs width vs. their frequencies. Both distributions of points can be well fitted by lines of slopes 0.390 for the fundamental, and 0.389 for the harmonic. The zero abscissa values are found to be  $-0.526052$  for the fundamental, and  $-0.932459$  for the harmonic (although their physical meaning is not clear). It is clearly visible on the plot that both QPOs are tightly correlated, the width of the harmonic being  $\sim$  twice that of the fundamental (resulting thus in a Q value ( $= \frac{\text{frequency}}{\text{FWHM}}$ ) similar for both).

## 5. Results and Interpretation

The April 17 observation confirms and expands the conclusion of Markwardt *et al.* (1999) and Munro *et al.* (1999), that the QPO frequency is better correlated with the soft flux, but seems stronger in the higher energy bands (which is confirmed by the following dates).

In addition a precise study of the lightcurve of the same date shows that the  $\sim 30$  min dips are smoothed with the

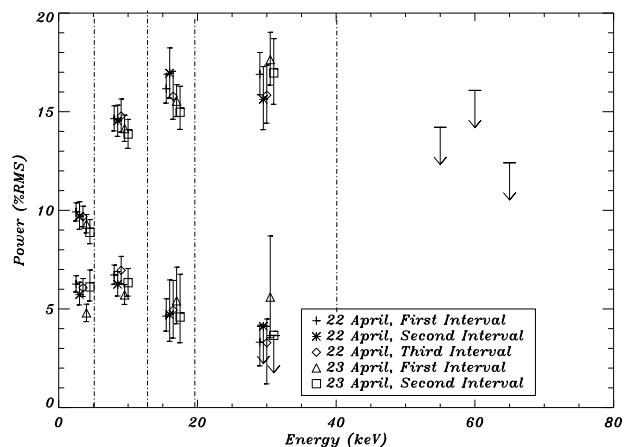


**Fig. 7.** Plot of the Power vs. the energy range; each group of points represents the value over the whole energy range delimited by the dash-dotted line. The upper group of points in each cases corresponds to the fundamental QPO, the lower being the harmonic. Error bars are  $1\sigma$  confidence level. Arrows are the 95% upper limits. The three last arrows represent, respectively, the result from Apr. 22 intervals 1 & 2 merged, Apr.22 interval 3, and Apr. 23 interval 1 & 2 merged.

energy, and that the sudden increase of the soft flux (the spike) is anti correlated with the hard flux; indeed the spike, in both interval, corresponds to a major decrease of the flux in the 20 – 40 keV, and 40 – 80 keV bands, usually considered to be emitted by the corona. The soft spike marks here the transition from the low hard state (C state of Belloni *et al.*, 2000), to a soft high state (A-B states). Within the interpretation in terms of disk states, this transition and the rapid variations following (interpreted as rapid transitions through A B C states (Belloni *et al.*, 2000)) can be seen as a succession of rapid replenishments and disappearances of the innermost parts of the disk (Belloni *et al.*, 1997). The behaviour of the corona may appear difficult to understand, since the abrupt cut-off of the hard X-rays could either be the manifestation of a sudden cooling of the relativistic electrons by the re-emergence of a high soft flux, or the disappearance of the corona (by advection or ejection).

Thanks to a large number of multi-wavelength observations, the radio and infra red behaviors of GRS 1915+105 have now been widely studied for years. In particular, former studies such as the one presented in Mirabel *et al.*, 1998, or Eikenberry *et al.*, 1998 had linked the soft X-ray spike (transition from low hard to soft high state) with radio and infra red flares. Dhawan *et al.* (2000) have shown that indeed superluminal ejections took place during abrupt change in the X-ray state of the source. More recently, Klein-Wolt *et al.* (2001) have found a strong correlation between radio events (radio oscillations, compact jets, large radio flares), and state C properties (duration, transition to other states). It is, however, to be noted that

Klein-Wolt *et al.*, did not find any simultaneous radio - alpha state observations. Furthermore, “The Largest Multi-wavelength Campaign” on GRS 1915+105 presented in Ueda *et al.* (2002), shows that the state transitions on Apr. 17<sup>th</sup> are followed by radio flares consistent with an ejection of material starting at the state transition. This leads us to suggest that the abrupt cutoff of the hard X-rays is more probably related to the disappearance of a part of the corona, blown away under the form of a synchrotron emitting blob of material detected in the infrared, and radio domains (fig. 1 and 2 in Ueda *et al.*, 2002). On the other hand, the behavior of the QPO and its harmonic at high energies poses severe constraints on theoretical models. The decrease of the QPO power above 40 keV may indicate that not all the corona is affected. The decrease of the harmonic above  $\sim 20$  keV also raises very challenging questions.

These could find an explanation in the context of the Accretion-Ejection Instability (Tagger and Pellat, 1999), which has been shown to form a rotating spiral structure in the disk, similar to galactic ones but driven by magnetic stresses rather than by self-gravity. The spiral arms should be expected to heat as well as compress the gas in the disk, and thus to appear as a rotating spiral or hot spot. The harmonic would then be a signature of the non-linear behavior of the spiral, just as the gas form shocks (and thus strong harmonics of the underlying 2-armed spiral) along galactic spiral arms. The high-energy cutoff of the fundamental could, then, favor an interpretation where most or all of the quasi-periodic modulation at high energies comes, not from the comptonized corona as usually assumed, but from a hot point in the optically thick disk. This would be consistent with the previous result (Rodríguez *et al.*, 2001; Rodríguez *et al.*, 2002) that the anomalously small color radius of the disk, often observed in some Black-Hole Binaries, could actually be interpreted by the black-body emission of a small area hot point in the disk. We could in principle have an estimate of its physical size, by adding a blackbody model in the spectral fits (such as the *BBODYRAD* model of XSPEC), one of the parameters being the normalized area of the emitting region, (since the black body luminosity is proportionnal to the area). But the limited sensitivity and spectral resolution of the present data do not allow any realistic fit. We expect that future instruments will provide better constraints on this problem.

It would be very tempting to consider the width of the QPO as a measure of the size (due for example to the differential rotation acting between the inner and outer edges of the spot). But the fact that we are dealing with a QPO probably rules out this explanation, since it has to result from a quasi-stationary feature in the disk. This is precisely the case for the AEI, where a standing spiral wave results in a quasi-stationary feature rotating at a single frequency. In this context the width of the QPO would correspond to the coherence time of this pattern, fixed either by non-linear effects or by variations in the background disk equilibrium, *e.g.* the inner disk radius or other

disk parameters (temperature, magnetization, etc.).

The spot physical properties (*e.g.* its temperature) may also depend on a number of external parameters, hard to deduce from the observations, such as the  $\beta$  ratio (the ratio between thermal and magnetic pressure), which drives the instability (see for example Varnière *et al.*, 2002, for a discussion on the effects of this parameter), or even the efficiency of the instability. Indeed, in a non linear regime for example, the amount of energy deposited in the disk (under the form of shocks) would be much greater, and would locally warm it up much more than in the linear case.

Further observational and theoretical work should, however, allow to test this hypothesis: by producing, from numerical simulations of the instability (such as Caunt and Tagger, 2001), synthetic light curves of the QPO, and by fitting the observed energy dependence of the modulated light curve by a high-temperature, hotter black body over a small area of the disk rather than the usual power-law of the coronal emission.

*Acknowledgements.* The authors would like to thank S. Corbel, M. Munro, P. Varnière, T. Foglizzo, and the anonymous referee for useful discussions and comments which allowed to improve the quality of the paper.

IFM acknowledges partial support from Fundación Antorchas. We also thank the *Athena help* at GSFC for appreciable help on the RXTE data reduction processes.

This research has made use of data obtained through the High Energy Astrophysics Science Archive Center Online Service, provided by the NASA/Goddard Space Flight Center.

## References

- Belloni, T., Méndez, M., King, A.R., van der Klis, M., van Paradijs, J., 1997, *ApJ*, **479**, L145.
- Belloni, T., Klein-Wolt, M., Méndez, M., van der Klis, M. and van Paradijs, J., 2000, *A&A*, **355**, 271.
- Castro-Tirado, A., Brandt, S., Lund, N., Lapshov, I., Sunyaev, R. A., Shlyapnikov, A. A., Guziy, S. & Pavlenko, E.P., *ApJS*, **92**, 469, 1994.
- Caunt, S. E., Tagger, M., 2001, *A&A*, **367**, 1095.
- Dhawan, V., Mirabel, I. F., Rodríguez, L. F., 2000, *ApJ*, **543**, 373.
- Eikenberry, S. S., Matthews, K., Morgan, E. H., Remillard, R. A., Nelson, R. W., 1998, *ApJ*, **494L**, 61.
- Greiner, J., Cuby, J. G., McCaughrean, M. J., Castro-Tirado, A. J., Mennickent, R. E., 2001, *A&A* **373L**, 37.
- Greiner, J., Cuby, J. G., McCaughrean, M. J., 2001, *Nature*, **414**, 522.
- Klein-Wolt, M., Fender, R.P., Pooley, G.G., Belloni, T., Migliari, S., Morgan, E.H., van der Klis, M., 2001 *MNRAS in Press* (astro-ph/0112044).
- Markwardt, C. B., Swank, J. H., Taam, R. E., 1999, *ApJ*, **513**, 37.
- Merloni, A., Fabian, A. C., and Ross, R. R., 2000, *MNRAS* **313**, 193 (**MFR**).
- Mirabel, I. F., Rodríguez, L. F., Cordier, B., Paul, J., Lebrun, F., 1992, *Nature*, **358**, 215.
- Mirabel, I. F., & Rodríguez, L. F., 1994, *Nature*, **371**, 46.

- Mirabel, I. F., Dhawan, V., Chaty, S., Rodríguez, L. F., Martí, J., Robinson, C. R., Swank, J., and Geballe, T., 1998, *A&A* **330**, L9.
- Mirabel, I. F., & Rodríguez, L. F., *Annu. Rev. Astron. Astrophys.*, **37**, 409, 1999.
- Morgan, E. H., Remillard, R. A., Greiner, J., 1997, *ApJ*, **482**, 1086.
- Muno, M. P., Morgan, E. H., and Remillard, R. A., 1999, *ApJ*, **527**, 321.
- Psaltis, D., Belloni, T., van der Klis, M., 1999, *ApJ*, **526**, 262.
- Rodríguez, J., Varnière, P., Tagger, M., Durouchoux, P., proceedings of the Third Microquasar Workshop: Granada Workshop on galactic relativistic jet sources, Eds A. J. Castro-Tirado, J. Greiner and J. M. Paredes, *Astrophysics and Space Science*, of the 3<sup>rd</sup> microquasar workshop, Granada (Spain), 2001 (astro-ph/0010635).
- Rodríguez, J., Varnière, P., Tagger, M., Durouchoux, P., 2002, *accepted in A&A*.
- Sobczak, G. J., McClintock, J. E., Remillard, R. A., Cui, W., Levine, A. M., Morgan, E. H., Orosz, J. A., and Bailyn, C. D., 2000, *ApJ*, **531**, 537 (**SMR**).
- Swank, J., Chen, X., Markwardt, C., and Taam, R., 1997, proceedings of the conference "Accretion Processes in Astrophysics: Some Like it Hot", held at U. Md., October 1997, *eds.* S. Holt and T. Kallman.
- Tagger, M., and Pellat, R., 1999, *A&A*, **349**, 1003 (**TP99**).
- Tagger, M., proceedings of the 5th Compton Symposium, Portsmouth (USA), 1999 (astro-ph/9910365).
- Ueda, Y., Yamaoka, K., Sánchez-Fernández, C., Dhawan, V., Chaty, S., Grove, J.E., McCollough, M., Castro-Tirado, A. J., Mirabel, L. F., Kohno, K., Feroci, M., Casella, P., Trushkin, S. A., Castaneda, H., Rodríguez, J., Durouchoux, P., Swank, J. H., Kotani, T., Ebisawa, K., 2002, *ApJ*, **in press**.
- Varnière, P., Tagger, M., Proceedings of the Gamma 2001 Symposium Baltimore MD, April 2001; N. Gehrels, C. Shrader, and S. Ritz, eds.
- Varnière, P., Rodríguez, J., Tagger, M., 2002, *accepted in A&A*.

Date	#	Energy range (keV)	$f_{QPO1}(Hz)$	$Q_1$	% $RMS_1$	$f_{QPO2}(Hz)$	$Q_2$	% $RMS_2$	$\chi^2$ (d.o.f.)
04 22 2000	1	PCA*	$2.148^{+0.006}_{-0.006}$	6.97	$12.47^{+0.62}_{-0.57}$	$4.242^{+0.019}_{-0.019}$	5.58	$6.31^{+0.48}_{-0.42}$	69.13(62)
		2 – 5 keV	$2.137^{+0.008}_{-0.006}$	7.12	$9.92^{+0.46}_{-0.46}$	$4.270^{+0.022}_{-0.02}$	5.34	$6.26^{+0.42}_{-0.4}$	89.2(62)
		5 – 13 keV	$2.142^{+0.007}_{-0.005}$	6.88	$14.64^{+0.65}_{-0.61}$	$4.249^{+0.019}_{-0.018}$	6.85	$6.72^{+0.50}_{-0.46}$	67.62(62)
		13 – 20 keV	$2.151^{+0.007}_{-0.006}$	6.68	$16.16^{+0.73}_{-0.73}$	$4.270^{+0.038}_{-0.038}$	7.89	$4.63^{+0.87}_{-0.76}$	62.11(62)
		20 – 40 keV	$2.143^{+0.01}_{-0.008}$	6.00	$16.89^{+1.10}_{-1.03}$	<i>4.27 frozen</i>	> 6.1	< 4.17	30.19(36)
	2	PCA	$2.161^{+0.007}_{-0.006}$	6.79	$12.27^{+0.78}_{-0.75}$	$4.305^{+0.024}_{-0.024}$	6.43	$5.39^{+0.57}_{-0.51}$	102.5(62)
		2 – 5 keV	$2.152^{+0.008}_{-0.007}$	7.24	$9.70^{+0.72}_{-0.66}$	$4.326^{+0.025}_{-0.025}$	6.21	$5.72^{+0.63}_{-0.52}$	108.6(62)
		5 – 13 keV	$2.162^{+0.006}_{-0.007}$	6.90	$14.53^{+0.79}_{-0.78}$	$4.286^{+0.024}_{-0.023}$	7.10	$6.24^{+0.64}_{-0.59}$	80.10(62)
		13 – 20 keV	$2.169^{+0.008}_{-0.009}$	5.60	$16.95^{+1.28}_{-1.26}$	$4.333^{+0.102}_{-0.092}$	5.82	$4.71^{+1.75}_{-1.35}$	87.52(42)
		20 – 40 keV	$2.182^{+0.012}_{-0.012}$	6.28	$15.62^{+1.66}_{-1.53}$	<i>4.30 frozen</i>	> 6.14	< 4.12	46.24(47)
	1 – 2 Merged	40 – 80 keV	<i>2.15 Frozen</i>	> 15	< 14.21				7.69(10)
	3	PCA	$2.378^{+0.008}_{-0.008}$	5.8	$12.31^{+0.70}_{-0.68}$	$4.654^{+0.029}_{-0.028}$	5.28	$5.94^{+0.55}_{-0.50}$	87.98(62)
		2 – 5 keV	$2.361^{+0.009}_{-0.008}$	5.84	$9.67^{+0.53}_{-0.5}$	$4.690^{+0.026}_{-0.025}$	5.39	$6.07^{+0.46}_{-0.43}$	94.8(62)
		5 – 13 keV	$2.382^{+0.008}_{-0.007}$	5.71	$14.78^{+0.86}_{-0.81}$	$4.691^{+0.03}_{-0.031}$	5.54	$6.95^{+0.7}_{-0.66}$	70.54(62)
		13 – 20 keV	$2.391^{+0.009}_{-0.009}$	5.97	$15.78^{+1.26}_{-1.16}$	$4.558^{+0.127}_{-0.1}$	6.16	$4.94^{+1.49}_{-1.42}$	100.1(62)
		20 – 40 keV	$2.376^{+0.013}_{-0.011}$	5.78	$15.83^{+1.52}_{-1.42}$	<i>4.65 Frozen</i>	> 5.8	< 4.48	43.58(36)
		40 – 80 keV	<i>2.35 Frozen</i>	> 10.21	< 16.08				19.29(28)
04 23 2000	1	PCA	$2.901^{+0.009}_{-0.007}$	4.77	$12.07^{+0.51}_{-0.47}$	$5.706^{+0.036}_{-0.036}$	4.42	$5.23^{+0.43}_{-0.35}$	87.98(62)
		2 – 5 keV	$2.871^{+0.009}_{-0.009}$	5.31	$9.30^{+0.48}_{-0.44}$	$5.832^{+0.041}_{-0.039}$	5.12	$4.80^{+0.44}_{-0.41}$	83.09(62)
		5 – 13 keV	$2.905^{+0.008}_{-0.007}$	5.12	$14.14^{+0.68}_{-0.65}$	$5.752^{+0.034}_{-0.033}$	5.70	$5.71^{+0.52}_{-0.48}$	79.32(62)
		13 – 20 keV	$2.921^{+0.01}_{-0.009}$	5.35	$15.53^{+0.84}_{-0.78}$	$5.535^{+0.132}_{-0.146}$	4.22	$5.48^{+1.71}_{-1.16}$	122.8(62)
		20 – 40 keV	$2.925^{+0.015}_{-0.015}$	4.91	$17.64^{+1.38}_{-1.29}$	$5.940^{+0.2}_{-0.16}$	7.36	$5.60^{+3.10}_{-2.06}$	76.89(59)
	2	PCA	$2.882^{+0.01}_{-0.008}$	5.34	$11.47^{+0.64}_{-0.54}$	$5.627^{+0.051}_{-0.051}$	3.91	$5.41^{+0.50}_{-0.47}$	100.1(62)
		2 – 5 keV	$2.866^{+0.012}_{-0.012}$	5.83	$8.88^{+0.64}_{-0.57}$	$5.714^{+0.067}_{-0.065}$	3.19	$6.11^{+0.85}_{-0.71}$	79.77(62)
		5 – 13 keV	$2.883^{+0.01}_{-0.009}$	5.49	$13.86^{+0.74}_{-0.72}$	$5.640^{+0.062}_{-0.063}$	3.90	$6.33^{+0.72}_{-0.68}$	94.63(62)
		13 – 20 keV	$2.899^{+0.013}_{-0.01}$	5.71	$14.97^{+1.31}_{-0.87}$	<i>5.65 Frozen</i>	4.92	$4.58^{+2.16}_{-1.3}$	63.84(42)
		20 – 40 keV	$2.901^{+0.019}_{-0.019}$	4.98	$16.96^{+1.73}_{-1.59}$	<i>5.65 Frozen</i>	> 17.65	< 3.65	36.86(29)
	1 – 2 Merged	40 – 80 keV	<i>2.85 Frozen</i>	> 7.5	< 12.41				50.04(41)

**Table 3.** results of the fittings for the three observations, for all the energy ranges defined in section 2. \*Instrument entire energy range ( $\sim 2 - 100$  keV).